Multimodal seismic assessment of infrastructures retrofitted with exoskeletons: insights from the Foggia Airport case study

(Article begins on next page)

02 May 2024

ORIGINAL ARTICLE

Multimodal seismic assessment of infrastructures retrofitted with exoskeletons: insights from the Foggia Airport case study

Raffaele Cucuzza[1] · Angelo Aloisio[2] · Marco Domaneschi[1] · Roberto Nascimbene[3]

Abstract

Addressing the seismic vulnerability of infrastructures is critical, especially for those built before the introduction of the current seismic regulations. One of the primary challenges lies in retrofitting these buildings without interrupting their functionality. In this context, the use of exoskeletons for seismic retrofitting represents an effective solution. This approach increases the seismic resistance and ensures the continuous operation of the building during retrofitting. This advantage is especially crucial for critical infrastructures, such as airports. Nevertheless, traditional seismic assessment methods based on pushover analyses might not accurately predict the seismic capacity of complex infrastructures dominated by local vibration modes. To bridge this gap, the study proposes refining the multimodal pushover analysis tailored for seismic vulnerability assessments of large infrastructures with exoskeletons characterized by low modal participation ratios. The Foggia Airport case study exemplifies these points and highlights the practical applications of the discussed advancements. The authors compared two force distributions for push-over analysis, addressing the fine-tuning of exoskeletons to maximize their seismic resistance.

Keywords Seismic retrofitting · Exoskeletons · Multi-modal pushover analysis

✉ Raffaele Cucuzza
raffaele.cucuzza@polito.it

Angelo Aloisio
angelo.aloisio1@univaq.it

Marco Domaneschi
marco.domaneschi@polito.it

Roberto Nascimbene
roberto.nascimbene@iusspavia.it

1 Department of Structural, Geotechnical and Building Engineering, Politecnico di Torino, Turin, Italy

2 Department of Civil, Construction-Architectural and Environmental Engineering, Università degli Studi dell'Aquila, L'Aquila, Italy

3 European Centre for Training and Research in Earthquake Engineering(EUCENTRE), Via Ferrata 1, Pavia, Italy

 🍊 Springer

1 Introduction

Recent seismic events have underscored the fragility of infrastructures in seismically active regions (Kawashima et al. 2009; Pang et al. 2020; Xiang et al. 2021; Salkhordeh et al. 2021). Many infrastructures were built before the adoption of contemporary European and International seismic guidelines (Wardhana and Hadipriono 2003; Afsar Dizaj et al. 2023; Zucca et al. 2023), leading to high seismic vulnerability (Wallace et al. 2001; Yen 2002). Ageing infrastructures, especially after the Morandi bridge collapse (Malomo et al. 2020; Calvi et al. 2019) and other events (Scattarreggia et al. 2022), are raising global concerns. To prevent future damages and losses, it is crucial to evaluate vulnerabilities and identify effective retrofitting solutions (Collura and Nascimbene 2023; Ghazal and Mwafy 2022; Markou 2021; Zanini et al. 2020; Reggia et al. 2020).

Recent studies have emphasized the benefits of seismic isolation or the introduction of dissipative devices as a primary retrofitting method (Cucuzza et al. 2023). This technique effectively reduces base shear, minimizes lateral drifts, and prevents inelastic deformations in the structure (Nestovito and Occhiuzzi 2016; Martelli et al. 2014). While seismic isolation is undoubtedly a valuable strategy, the uninterrupted operation of critical infrastructures, such as commercial hubs and airports, is paramount during seismic retrofitting. Therefore, for vital facilities, alternative solutions like external structures, including exoskeletons (Di Lorenzo et al. 2020; Formisano and Messineo 2022), rocking walls (Di Egidio et al. 2020, 2021, 2023), are more appropriate to guarantee continuous functionality.

Historically, seismic retrofitting interventions were based on steelwork (Mazzolani 2007). However, in recent times, alternative materials and techniques have come to the forefront, gradually replacing steel-based systems (Rowe and Walther 1993; Agency 2006). Still, in scenarios where it is imperative to conduct external-only modifications without compromising the building functionality, steel exoskeletons represent an optimal choice (Bellini et al. 2018; Caverzan et al. 2016; Foraboschi and Giani 2017, 2018; Landolfo et al. 2021; Barbagallo et al. 2022). Exoskeletons improve the whole building, from its aesthetics and capacity to its impact on the environment (Marini et al. 2014, 2015, 2017). Such interventions proved their effectiveness in several experimental tests and during earthquakes (Foutch et al. 1989; Kaltakci et al. 2008; Wada et al. 2010; Görgülü et al. 2012).

Exoskeletons have been used on various structures, but their application to airports is rare. This study presents a case study where steel exoskeletons are employed for seismic retrofitting an existing airport in Foggia (Italy). The authors address the optimization of the in-plane configuration of the exoskeletons using multiple strategies addressing the influence of local modes on the seismic response. One of the significant challenges, besides the structural optimization, is accurately assessing the seismic performance. Given that these structures exhibit prevalent local modes, conventional uni-modal pushover analysis can lead to biased assessments.

Pushover analysis is a standard nonlinear method for assessing structural performance. Traditionally, this method focuses on the first mode and overlooks the effects of higher vibration modes (Habibi et al. 2022). Pushover analysis generally requires applying a lateral force pattern corresponding to the first mode. However, this assumption has several limitations, particularly in buildings with dynamic responses dominated by the higher modes (Saiidi and Sozen 1981; Fajfar 2000). As a result, its primary application is for low-rise buildings, necessitating adjustments for taller structures to consider higher-mode effects. Given these limitations, many researchers attempted to improve pushover analyses accounting for higher vibration modes. For instance, Sasaki et al. (1998) introduced

the multi-mode pushover (MMP). Other methodologies, like the modal pushover analysis (MPA) by Chopra and Goel (2002), also used varied load patterns related to each mode shape. However, some methods do not account for variations in the structural stiffness (Kalkan and Kunnath 2007). Thus, adaptive pushover methods have emerged, such as the adaptive modal combination (AMC) (Kalkan and Kunnath 2006), which integrates adaptive mode-based force patterns. Some researchers, like Antoniou and Pinho (2004), compared the accuracy of adaptive vs. non-adaptive techniques, while others, like Mao et al. (2008), enhanced existing modal pushover analyses. There have been continuous efforts to enhance pushover analysis accuracy, with numerous studies proposing new lateral load patterns (Chen et al. 2014; Amini and Poursha 2018; Bergami et al. 2020).

Still, while various methodologies exist in pushover analysis, the prevailing focus in much of the research remains on the load pattern. A significant gap in the literature pertains to the optimal transformation factor for converting the multi-degree of freedom (MDOF) system to the single-degree of freedom (SDOF) system, especially when dealing with a multimodal force distribution. This topic is contentious and requires more attention from scholars.

This paper examines a case study where the local modes play a primary role, and the first mode is not well representative of the building's dynamics. The study first compares two force distributions: one derived from a modal combination and the other uniformly proportionate to masses. They then adopt a novel approach for scaling the MDOF to SDOF, having evaluated and compared multiple transformation factors for model reduction. Therefore, in addition to presenting this peculiar case study on seismic retrofitting using exoskeletons, this work addresses specific flaws of standard multimodal pushover analysis.

The paper's structure is as follows: beginning with an introduction to the case study, the authors discuss the seismic retrofitting measures and the procedures for vulnerability assessment, considering loads and seismic demand. A subsequent section on exoskeleton optimization determines the ideal configuration. The paper then evaluates seismic vulnerability pre and post-retrofit using the multi-modal pushover method. Before this, the authors outline the limitations of current methods, suggesting a refined approach for pushover analyses.

2 Case study description: the Foggia Airport

Established in 1968 for civil purposes, the Foggia Airport has intermittently served as a critical hub for commercial flights in the northern part of Puglia (Italy). Given the growth in activities at the airport, local authorities felt the urgency to commission a seismic vulnerability assessment and retrofitting measures. This initiative aims to ensure uninterrupted operations and provide the utmost safety for its users while achieving an architectural rehabilitation of the entire building.

2.1 As-built structure

The Foggia Airport consists of a steel moment resisting frame without additional lateral resisting systems (NEHRP 2006). The building has three floors, each with a different weight distribution. The raised floor carries much more of the loads than the other floors as it accommodates the entire flow of passengers. It is located 1.40 cm respect the ground

Fig. 1 **a** Front view of the main entrance. **b** Perspective view of the air-side
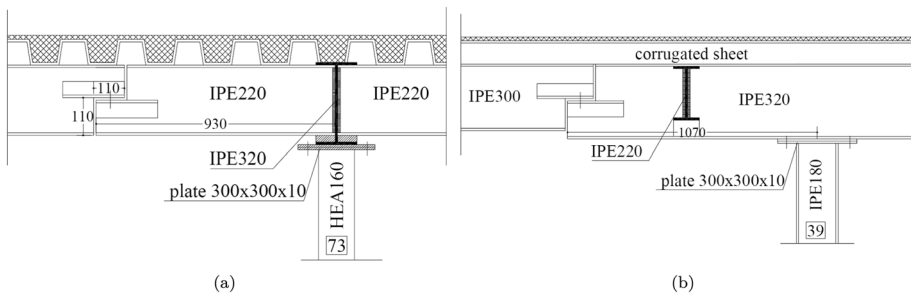

Fig. 2 Detail of the columns-main beams (**a**) and columns-secondary beams (**b**) connection supporting the deck of the raised floor. Measures are expressed in millimeters

level in fact stairs along the entire perimeter of the building were realized to cover this gap in elevation. The second floor has two main parts: one section supports a corrugated sheet roof made of a 10 cm steel deck filled with concrete (approximately 80% of the entire footprint), and the remaining area is used for executive offices. The third floor mainly acts as a protective cover for the offices below.

The Foggia Airport covers an area of roughly 2960 m², with 320 m² dedicated to executive spaces on the + 6.15 m level. The total height measured with respect to the ground floor is 10.40 m (Fig. 1).

The steel moment-resisting frames consist of HEA 160, mainly adopted for the realization of the short columns supporting the ground floor, and HEA 180 profiles as supports of the roof above the first and second floor. The main truss beams are connected to the columns, while secondary beams hinge on primary ones; see Fig. 4. Specifically, half-joint connections (Rosso et al. 2022) were realized in situ to guarantee the continuity of both main and secondary beams. Above, the first storey at + 1.4 m has a thin steel deck slab, realized by a composite system of corrugated sheet (see Fig. 2) and concrete upheld by IPE 320 and/or IPE 300 beams adopted for the main beams and IPE 220 for the secondary ones.

The subsequent levels employ several truss beams obtained from assemblages of double angles and IPE sections. The second storey (see Fig. 3), elevated at + 6.15 m, mainly serves as a roof, except for a portion of internal offices. The slab, similar to that in executive
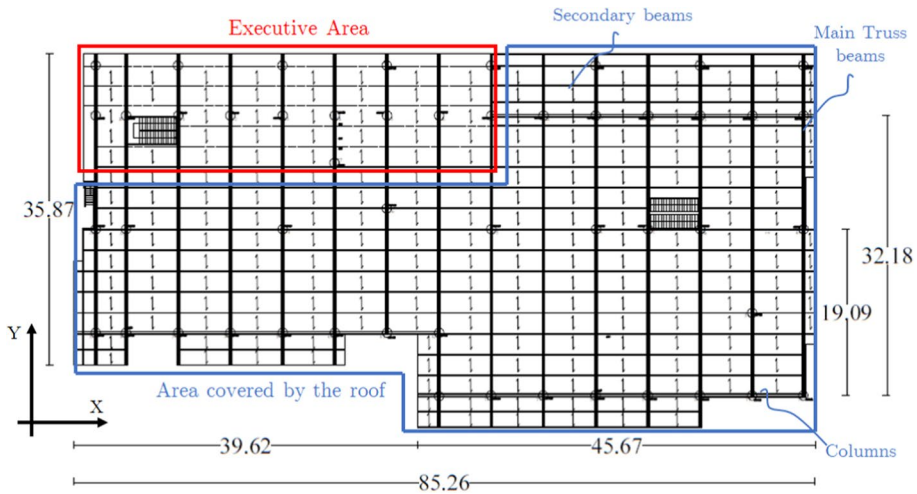
Fig. 3 Layout of the second floor + 6.15 m

zones and atop the structure, adopts a lean steel deck design similar to the roof system of industrial buildings.

As depicted in Fig. 3, the geometrical scheme intended as positions of vertical and horizontal elements is similar for both the ground and first floor. More in detail, consecutive main and secondary beams are located at 6.0 m and 2.5 m each other, respectively. However, despite the columns supporting the raised floor which are placed in correspondence of each connection joint between the main and secondary beams, vertical elements of the raised floor exhibit variable length spans ranging from 5.0 up to 30.0 m . Obviously, the need to cover larger roof spans is peculiar to this type of strategic building so as to ensure maximum functionality during the activities of the airport. Specifically, the truss beams along the y-direction, which cover the airport area dedicated to the security service and preliminary passenger screening, show the most critical span.

The beam-to-column connections with welded plates allow for some bending moment transfer. Additionally, several connections, see Fig. 4b, lacked professionalism, perhaps due to transportation challenges during construction.

2.2 Geometric and structural survey

The concept of"knowledge level"is fundamental when dealing with existing structures, rehabilitations, or retrofit projects. It pertains to the amount and quality of information available about a structure, encompassing its design, construction, material properties, previous modifications, and current condition.

Three primary factors influence the determination of knowledge level: (1) documentation: availability and comprehensiveness of original design drawings, as-built records, construction notes, and any subsequent modifications. (2) Physical inspection: a detailed assessment of the structure, which includes visual inspections and non-destructive testing. (3) Material testing: in some cases, invasive testing is needed to determine the condition and properties of materials, connections, and elements.
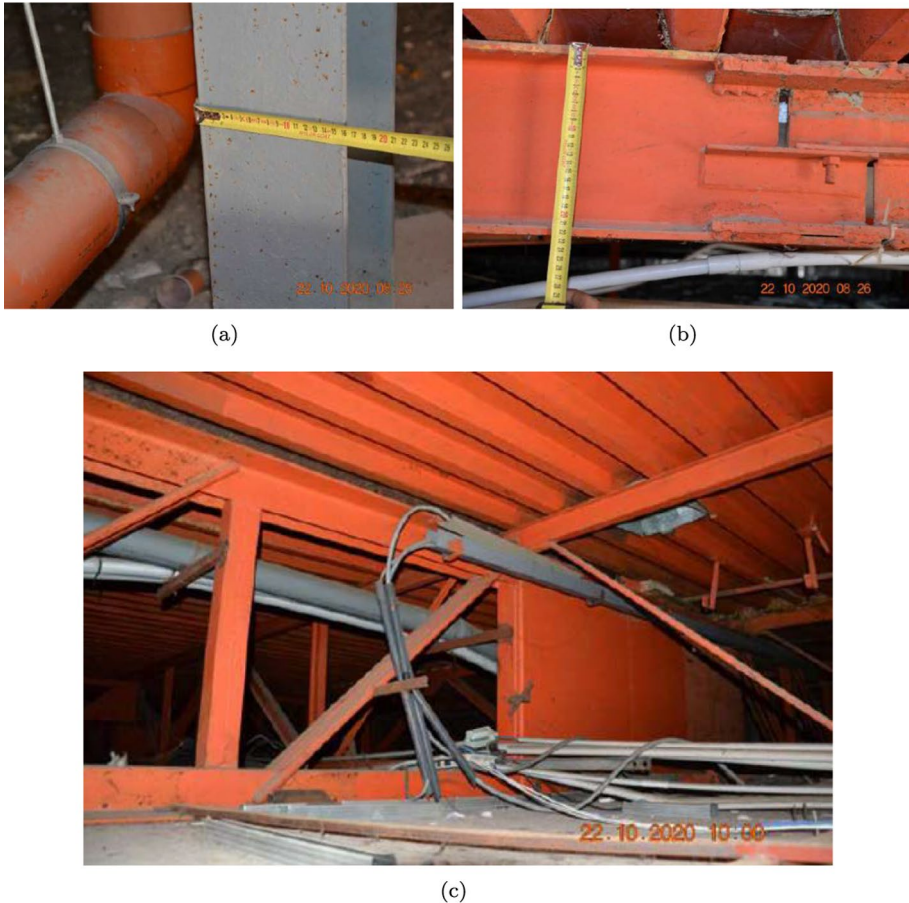
(a)

(b)

(c)

Fig. 4 **a** HEA160 short column supporting the raised floor; **b** detail of a hinged connection at the raised floor level; **c** close-up of a rigid connection on the primary truss beams

Based on the combined insights from these sources, an engineer can classify the structure into specific knowledge levels. This classification can then guide the subsequent analysis, design decisions, and safety evaluations, ensuring that the structure meets current standards and safety requirements. According to the Italian standard, there are three knowledge levels: minor, moderate, and extensive, labelled LC1, LC2, and LC3, respectively.

The Italian standards highlight three primary criteria for determining the knowledge level (LC) for steel structures: (1) presence of original and exhaustive as-built record drawings. (2) detailed survey covering elements and connections. (3) Verification of element mechanical properties. According to the Italian code, at least three samples per 300 m^2 of storey's footprint are required for a survey to be classified as extensive (LC3), covering both main elements and connections. By this metric, the survey aligns well with the LC3 knowledge level. Nonetheless, the final designation has been at LC2 due to the lack of original drawings and ambiguities in the typology and position of certain connections, especially at the raised floor and roof levels. Additionally, either the presence of an unusual

assemblage of steel pieces so far to the current practice and the impossibility of extending the geometric survey to all the structural elements suggests a more conservative approach

A comprehensive geometric survey was conducted, and tensile tests on steel samples revealed an average yield resistance of 290 MPa for steel members. This indicates that the predominant steel type aligns with the S275 category per European standards. Tests conducted on the welded plates indicated a steel type consistent with S355. The foundation elements have a thick concrete cover that restricts rotation, acting like stiffened connections. According to this result, the foundation will be not considered in the modelling. Additionally, no corrosion was found on the elements.

With LC2, the confidence factor FC for assessing the design strengths must be set at 1.2. Thus, the steel design strength values (f_{yd}) are

$$f_{yd} = \frac{f_y}{FC} = \frac{275\,\text{MPa}}{1.2} = 229.16\,\text{MPa} \qquad (1)$$

2.3 Load evaluation

The load evaluation for the Foggia Airport structure was conducted to ensure compliance with Italian standards. Table 1 shows the gravitational loads acting on different sections of the airport structure. The loads are divided coherently with their nature:

- G1 represents the permanent load due to structural components like slabs and decks.
- G2 identifies permanent non-structural loads.
- Q denotes variable loads, such as airport traffic for the rising floor or office-related loads for administrative sections, maintenance and snow loads for the planar roofs.

The primary lateral forces come from wind and earthquake hazards.

Wind loads are dynamic forces that can significantly affect the stability and safety of a structure, especially in open areas like airports. Table 2 presents the key parameters to determine the equivalent static wind loads on the Foggia Airport structure recommended by the Italian Code.

Table 1 Gravitational load evaluation

Floor/area	Load type	Value (kN/m²)
Raising floor	Concrete slab (G1)	1.5
	Permanent (G2)	2.0
	Airport traffic (Q)	5.0
Administrative offices	Concrete slab (G1)	1.25
	Corrugated deck (G1)	0.2
	Permanent (G2)	2.0
	Airport offices (Q)	3.0
Roof top	Roof of concrete (G2)	1.3
	Corrugated deck (G2)	0.2
	Roof maintenance (Q)	0.5
	Snow (Q)	1.0

Table 2 Wind load parameters

Parameter	Value
Air density (kg/m^3)	1.25
Wind speed (vb,0) (m/s)	27
Wind pressure (qb) (kN/m^2)	0.456
Wind pressure factor Cpe(0.4) (kN/m^2)	0.174
Wind pressure factor Cpe(0.8) (kN/m^2)	0.348

Regarding the seismic action, following Italian regulations, the authors undertook seismic assessments with an elastic response spectrum based on pseudo-acceleration and a 5% damping ratio. This spectrum corresponds to the life safety limit state (SLV). The design spectrum has been scaled using a behaviour factor of 1.5 for the as-built structure and 1 for the retrofitted structure. While the as-built steel structure, as later shown, preserves small ductility sources, the retrofitted one has none.

Expressly, the as-built structure has limited ductility sources and vulnerability to brittle failures, evident from the short columns on the raised floor and the absence of bracings. According to the code, the airport has been assigned a nominal lifespan of 50 years (building with ordinary performance level) and is categorized under usage class III. Though strategic buildings like airports are usually categorized under class IV, in this specific case the Foggia airport represents a secondary hub with respect to the principal one located in the regional capital (i.e. Bari). Moreover, at the present time, the limited number of passengers hosted by the building makes the choice a reasonable assumption.

Table3 presents the elastic spectrum parameters as per Italian seismic regulation.

2.4 FE modeling

The main structure consists of 15 frames in the *y*-direction and 17 in the *x*-direction, as shown in Fig. 5.

The authors did not model the control tower. The tower does not meet essential safety and stability standards, making demolition a likely option. Because of these issues, most modelling approaches suggest not including the tower in the structural analysis. This decision is backed by a recent rule from the ENAC (Italian Civil Aviation Authority), which now allows control towers to be built separate from the main airport building.

Table 3 Parameters of elastic spectrum as per Italian seismic Regulation

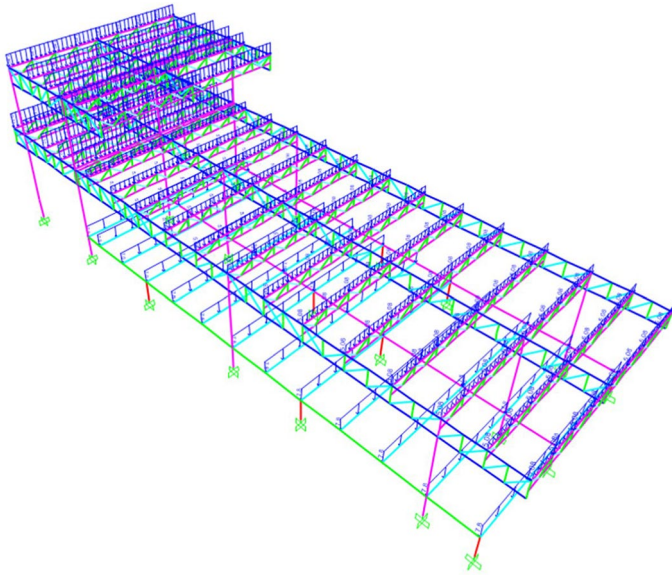| Parameter	Value
Town	Foggia
Function critical damping ratio	5%
Usage class	III
Nominal life (years)	50
Peak ground acceleration ag/g	0.1572
Amplification factor, F0	2.6
Reference period Tc*	0.4396
Soil type	D
Topography class	T1

Fig. 5 View of a FE model module-type indicating the applied vertical loads acting on the main beams according to the floors' warping

The stories do not meet the slab thickness requirements as per Italian regulations, showing flexibility. Therefore, rigid body behaviour was not adopted for the floors as well as *shell* elements were avoided. Issues arose with mesh refinement between shell and frame elements, leading to stability problems. Hence, the authors applied equivalent loads directly to frames. However, with the aim to simulate the low constraint level exhibited by the deck, dummy beams with zero masses and low stiffness have been modelled as virtual bracings lying on the horizontal plane of the slab. All the structural elements composing the main and secondary truss beams as well as the beams lying on the raised floor and the columns have been modelled by using the *beam* element of SAP2000. Elastic hinges have been modelled in correspondence of the half-joint connections and column-beam connections detected during the survey.

The structural nonlinearities have been lumped in the plastic hinges at the end of beams and columns. Typically, these hinges appear at the beam ends before manifesting in columns. The study utilized the plastic hinge guidelines set by FEMA-356 and ASCE 41-13, tailored for steel structures. These hinges account for axial force interactions and have a length corresponding to the height of the member's cross-section.

3 Seismic retrofitting using exoskeletons

The structure under consideration exhibits a limited dissipating behaviour. Given the challenges of increasing the dissipation sources while maintaining the operational infrastructure, exoskeletons represent a valid solution. Moreover, adherence to guidelines set by the airport administration is paramount. Specifically, the design has prioritised preserving the facades of the main entrances and the bus arrival area.

The authors aimed to reduce the structure's displacements by strategically placing a series of exoskeletons around the base perimeter. While the optimal placement of exoskeletons can effectively reduce torsional effects and improve structural performance, an overabundance might stiffen the structure excessively, potentially amplifying seismic forces. It should be remarked that the exoskeletons are intended to rest on a foundation system distinct from the primary structure.

As depicted in Fig. 6, the exoskeleton under consideration is characterized by a triangular geometry characterized by intrinsic robustness and rigidity deriving also from the arch shapes of the three vertical chords. This structure is designed with a tiered approach, each level decreasing in size as it progresses upwards, with a tapering profile. Its cross-braces are integral to the triangular configuration, contrasting the lateral forces. In Fig. 6b, the pink elements indicate the primary vertical members while in red the secondary horizontal ones.

The exoskeleton's dimensions, depth and width are related to the building's height. The depth is half the building's height; see Fig. 6. The radius was chosen to quadruple the depth of the exoskeleton aiming to give more stability in either the main directions as well as ensuring an efficient arch behavior of the main chords. While arches with reduced radii might demonstrate enhanced performance, they demand increased depth in the exoskeleton, potentially leading to a disproportionate retrofit.

During the design of these specific external retrofitting structures, the connections with the existing building play a crucial role. Only with well-realized connections the coupled system can work efficiently and preserve the reference structure by simultaneously unloading the existing building and capturing the majority of the horizontal seismic actions. The exoskeletons will be rigidly anchored to the top and bottom chord of the truss beams at each level of the building's floor. Specifically, column-beam connections have been preferred to guarantee the best transfer path of the load. The structural redundancy of the connection, vitally important during a seismic event, and an adequate stiffness level has been assured by a truss system shown in Fig. 6b.
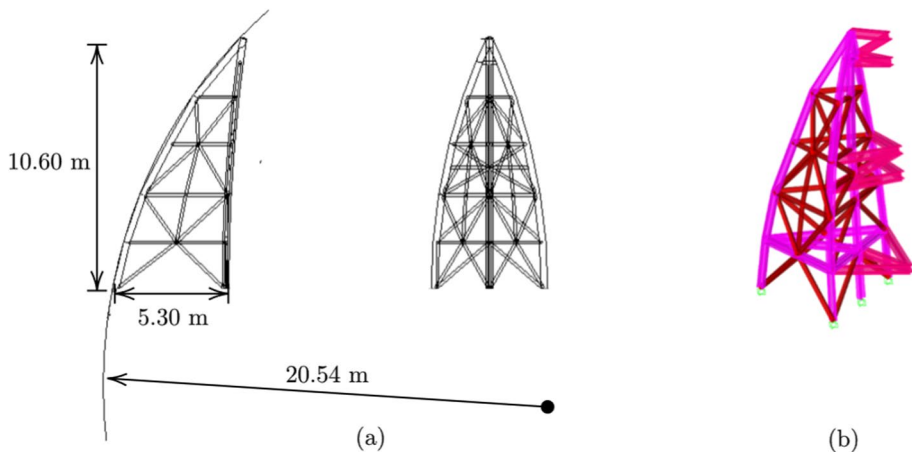

Fig. 6 **a** Design parameters of the exoskeletons and **b** related FE model

3.1 Sensitivity of the modal parameters to the exoskeleton position

The structural survey identified the lack of horizontal bracings, which hindered the assumption of a rigid body. A lack of rigid in-plane behaviour can undermine the force transfer between the structure and the exoskeletons. Therefore, the authors, before assessing the sensitivity of the modal parameters to the exoskeleton's position, first attempted to improve the in-plane stiffness using in-plane bracings. The position of the bracings aimed to increase the mass participation factors in the orthogonal directions. Figure 7 displays the chosen bracings configuration based on functional and architectural needs.

Given the configuration with improved in-plane stiffness, the authors assessed the modal parameters' sensitivity to the exoskeletons' placement.

Achieving global behavior of the coupled system with few fundamental modes associated with significant mass participation factors represents the final aim of this preliminary investigation.

During the initial phase, exoskeletons were positioned along the primary axes of the structural frames, with their placement influenced by non-structural elements. The final configuration of these exoskeletons does not follow a fixed method, evolving through iterative adjustments, considering the number of exoskeletons, their locations, and the properties of their cross-sections.

The authors analyzed five different exoskeleton configurations, highlighting how modal parameters are affected by the positioning of the exoskeletons. While exoskeletons increase structural stiffness, they could unintentionally push the structure into a zone of high acceleration in the elastic response spectrum. Furthermore, these exoskeletons aim to limit the number of local modes, ensuring that the main modes' cumulative mass participation ratio stays at or above 85%.

Figure 7 displays the considered five configurations investigated at this stage. The external arch exoskeletons added to the main structure exhibit distinct positions in the five configurations. In the first configuration, the exoskeleton arches are evenly distributed along the perimeter of the main structure. They extend outward symmetrically on both sides of the structure, parallel to the plane. This first attempt presents several issues mainly related to the obstacles provided by the exoskeletons along the air-side of the airport. However, the investigated scenario fails to achieve satisfactory global behaviors due to the presence of several local modes mainly chargeable to the perimeter elements of the existing buildings between consecutive exoskeletons. In the second configuration, similar to the first configuration, the exoskeleton arches are also uniformly distributed but extend outward asymmetrically. They are concentrated on the principal facade while the area of the airside, devoted to the passengers' transport, is not constrained. It is worth noting that in the
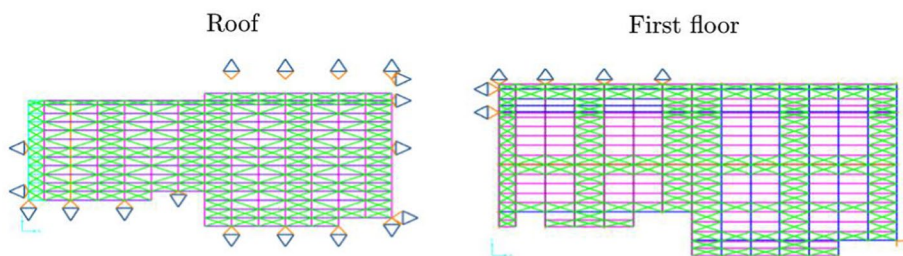

Fig. 7 Optimal bracings placement in the final configuration

second scenario, the number of fundamental modes along the x-direction is reduced to two with significant mass participation factors. As expected, an increase of the local modes's number along the y-direction is recognized. The third, fourth and fifth configurations are characterized by slight modifications in the final arrangement of the exoskeletons aiming to respect the constraints on the main facade (i.e. main entrances) and on the air-side. In the last configuration, though the number of exoskeletons is dramatically reduced with respect to the first scenario, an improvement in terms of both the numbers of vibration modes and the significance of corresponding mass mobilization can be observed as reported in Table 4. It is worth noting that the high-order modes assessed for the last configuration are mainly determined by vibrations of a few elements (eternal beams) lying on the raised floor (Fig. 8).

Table 4 reports the modes characterized by the highest modal participation ratios for the five configurations in the x and y directions. In almost all configurations, the first mode tends to dominate the x direction, with almost 70% mass participation ratio. For the y direction, modal participation varies across configurations. As expected, by decreasing the number of exoskeletons, high-order modes appear and the first one becomes less dominant (from 50% of the 1st configuration to 26% of the 5th configuration). Interestingly, the addition of exoskeletons leads to an increment of the number of modes necessary to achieve 85% of the mass participation. The base structure was initially analyzed for 40 vibration modes, capturing a minimum of 85% of the modal mass participation. In contrast, the coupled system model required a minimum of 250 vibration modes to achieve the same level of participation.
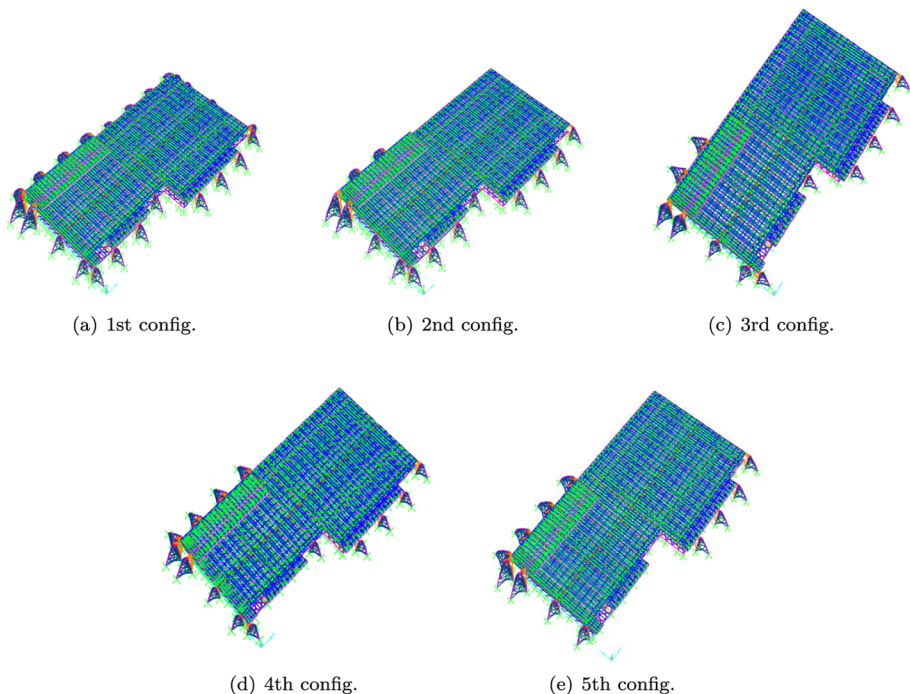

(a) 1st config.   (b) 2nd config.   (c) 3rd config.

(d) 4th config.   (e) 5th config.

Fig. 8 Considered five configurations of the exoskeletons

Table 4 Modal participation ratios of the five structural configurations in the x (Ux) and y (Uy) directions, with T the fundamental period and $S_a(T)$ the related spectral acceleration

Configuration	Direction	T [s]	$S_a(T)$ [g]	Uy	Ux
1st configuration	y-dir. Mode No. 208	0.164	0.548	0.504	–
	y-dir. Mode No. 40	0.251	0.689	0.212	–
	y-dir. Mode No. 190	0.194	0.595	0.075	–
	y-dir. Mode No. 170	0.215	0.631	0.046	–
	y-dir. Mode No. 169	0.216	0.632	0.040	–
	x-dir. Mode No. 1	0.306	0.730	–	0.683
	x-dir. Mode No. 36	0.254	0.694	–	0.104
	x-dir. Mode No. 18	0.268	0.717	–	0.080
2nd configuration	y-dir. Mode No. 210	0.168	0.553	0.409	–
	y-dir. Mode No. 4	0.297	0.730	0.207	–
	y-dir. Mode No. 209	0.169	0.556	0.062	–
	y-dir. Mode No. 2	0.354	0.730	0.040	–
	y-dir. Mode No. 218	0.150	0.525	0.039	–
	y-dir. Mode No. 138	0.236	0.665	0.038	–
	y-dir. Mode No. 211	0.165	0.549	0.026	–
	y-dir. Mode No. 23	0.267	0.715	0.024	–
	y-dir. Mode No. 204	0.170	0.557	0.024	–
	x-dir. Mode No. 1	0.402	0.730	–	0.622
	x-dir. Mode No. 3	0.322	0.730	–	0.270
3rd configuration	y-dir. Mode No. 203	0.174	0.564	0.375	–
	y-dir. Mode No. 4	0.314	0.730	0.144	–
	y-dir. Mode No. 2	0.366	0.730	0.108	–
	y-dir. Mode No. 204	0.174	0.562	0.101	–
	y-dir. Mode No. 211	0.167	0.551	0.044	–
	y-dir. Mode No. 5	0.292	0.730	0.042	–
	y-dir. Mode No. 202	0.175	0.566	0.032	–
	y-dir. Mode No. 201	0.176	0.567	0.031	–
	x-dir. Mode No. 1	0.407	0.730	–	0.611
	x-dir. Mode No. 3	0.324	0.730	–	0.272
4th configuration	y-dir. Mode No. 201	0.174	0.564	0.413	–
	y-dir. Mode No. 3	0.313	0.730	0.246	–
	y-dir. Mode No. 202	0.174	0.564	0.117	–
	y-dir. Mode No. 199	0.176	0.567	0.031	–
	y-dir. Mode No. 6	0.289	0.730	0.030	–
	y-dir. Mode No. 209	0.166	0.551	0.023	–
	x-dir. Mode No. 1	0.390	0.730	–	0.695
	x-dir. Mode No. 2	0.318	0.730	–	0.205

Table 4 (continued)

Configuration	Direction	T [s]	$S_a(T)$ [g]	Uy	Ux
5th configuration	y-dir. Mode No. 2	0.338	0.730	0.257	–
	y-dir. Mode No. 210	0.166	0.551	0.214	–
	y-dir. Mode No. 195	0.189	0.588	0.188	–
	y-dir. Mode No. 179	0.211	0.623	0.095	–
	y-dir. Mode No. 4	0.292	0.730	0.038	–
	y-dir. Mode No. 191	0.196	0.600	0.029	–
	y-dir. Mode No. 193	0.193	0.595	0.027	–
	x-dir. Mode No. 1	0.399	0.730	–	0.647
	x-dir. Mode No. 3	0.323	0.730	–	0.261

However, even if the last configuration seems to maintain a reasonable number of vibration modes with significant mass mobilization if compared with configurations in which a limited number of exoskeletons have been considered, the structural efficiency is not satisfactory. The total shear base capture by the exoskeletons does not achieve 30% of the total seismic demand in all the investigated scenarios. The optimal configuration should almost totally unload the base structure to guarantee structural safety under horizontal forces.

For this reason, the optimal configuration obtained, by considering this aspect, is reported in Fig. 9.

The peculiarity of this configuration consists of the presence of short exoskeletons along the area devoted to the main entrance of the airport. In this way, the architectural and logistic constraints imposed by the clients have been respected. Moreover, the local modes along the y-direction shown for the fifth configuration disappeared and an integral behavior of the coupled system was achieved.

Finally, as demonstrated by the results of the nonstatic analysis reported in the next section, 50% of the total seismic demand is captured by the external retrofitting systems.

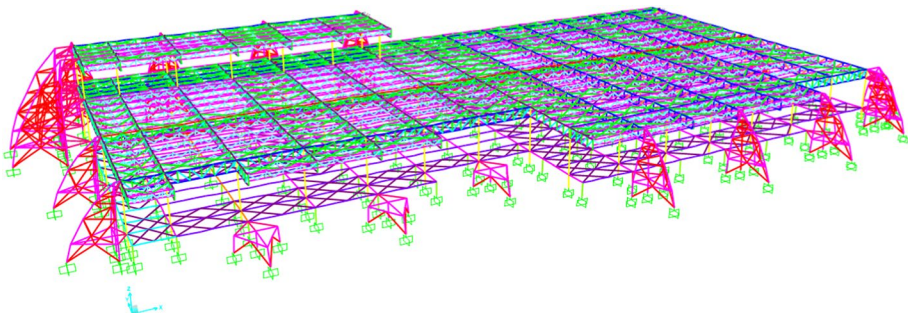Table 5 reports the cross-section properties of the exoskeletons in the optimal configuration.

Fig. 9 View of the optimal placement of the exoskeletons in the final configuration

Table 5 Cross section properties of exoskeletons in the optimal configuration

Type of element	Cross section	Area (mm^2)	Fyd (MPa)	Axial capacity (kN)
Main arcs	HEB260	11,800	350	4,130
Skeleton bracings	Circular hollow (219.1×5)	3363	350	1177
Links	HEB260	11,800	350	4130

In this preliminary stage, it could be interesting to observe how the modal shapes change after the retrofitting aiming to assess the goodness of the proposed intervention. Either the in-plane bracings or the exoskeletons lead to an integrated behavior of the coupled structure with few fundamental frequencies associated to significant mass participation factors as shown in Fig. 10.
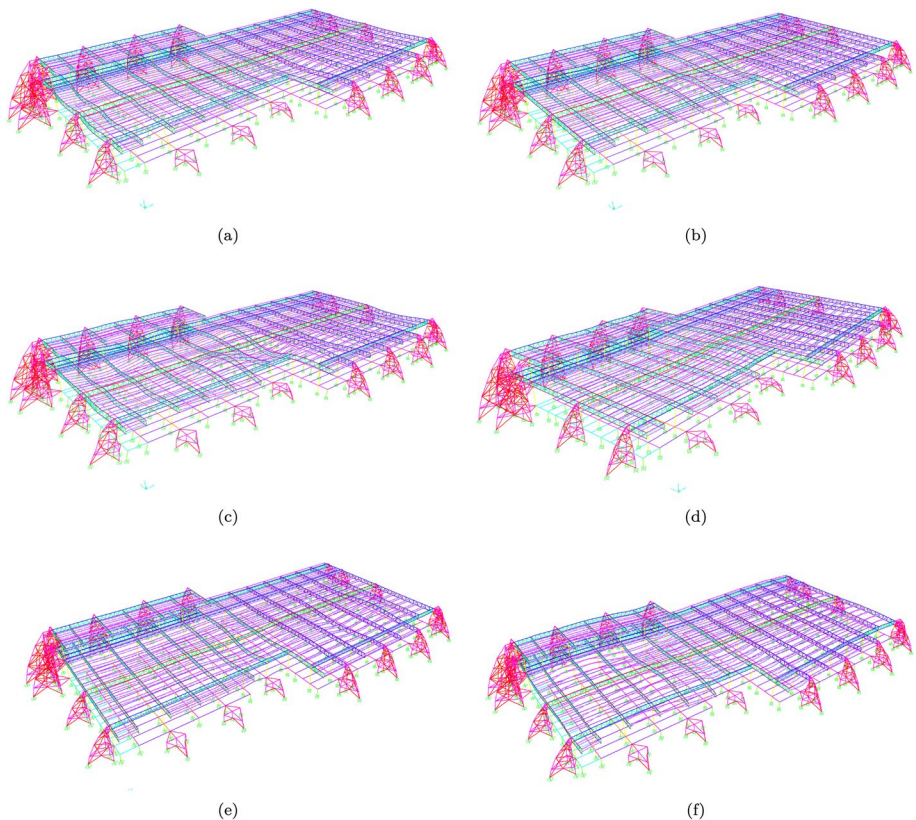

(a) (b)

(c) (d)

(e) (f)

Fig. 10 Representation of the three fundamental modes with the most significant participation mass factors along x-direction (**a**–**c**) and y-direction (**d**–**f**) for the best retrofitting scenario

4 Seismic performance evaluation

4.1 Linear dynamic analysis

Linear dynamic analyses with seismic response spectra have been carried out. Specifically, the structural analysis comprised the following sub-phases:

1. Determine the response spectrum: compute the design response spectrum based on the site-specific hazard parameters specified by the Italian Seismic code.
2. Conduct linear dynamic analysis and assess seismic demand: apply the response spectrum and estimate the seismic demand for all structural elements. The demand is computed through modal superposition, using the complete quadratic combination (CQC) method (Humar 2012), as per Italian Standards.
3. Evaluate building's capacity: calculate the seismic capacity of all structural elements. The capacity of the building corresponds to the minimum capacity among all structural elements. The capacity for each structural element is calculated from the analytical expressions specified in the Italian Code (e dei Trasporti 2008), aligning closely with the Eurocodes.
4. Compute the seismic vulnerability index, obtained as follows:

$$\zeta_E = \min\left\{ \frac{C_1}{D_1}, \frac{C_2}{D_2}, \dots, \frac{C_n}{D_n} \right\} \tag{2}$$

   Here C_i and D_i indicate the capacity and demand of the ith structural element, respectively.
5. Progressively scaling the response spectrum and repeating steps No.2-4 in order to identify the structural element associated with the first failure. This step provides evidence of the most vulnerable structural elements requiring specific care in the retrofitting; see Fig. 11.

   The authors compared the vulnerability indexes obtained from linear dynamic analyses and pushover analysis, outlined in the following subsection, highlighting the pros and cons of the two evaluation methods.
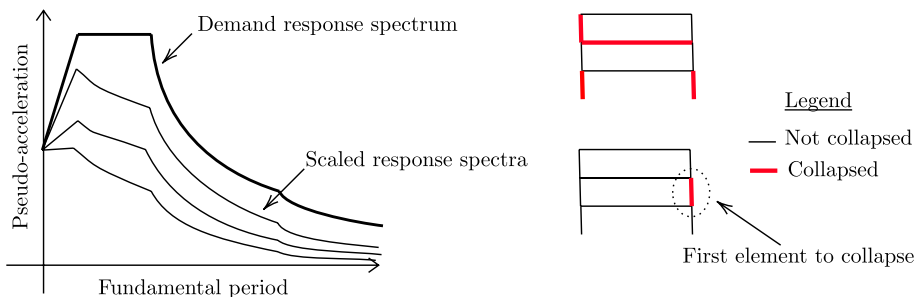

Fig. 11 Illustration of the scaling procedure of the design spectrum to identify the first structural element to fail

4.2 Non-linear static analysis background

The seismic assessment of the retrofitted structure has been based on nonlinear pushover analyses (Fajfar 1996). There are multiple pushover methods, each with strengths and weaknesses. At the core of conventional pushover analysis is the assumption that a single mode predominantly influences the structural response and remains unchanged throughout the structural performance. Many studies have confirmed that such an approach provides reasonably accurate estimates of the seismic response in MDOF systems only when the first mode dominates the response.

To investigate the structural behaviour when the higher modes are significant, many variants of unimodal procedures have been proposed, adopting load profiles derived from the mode shape combination. Therefore, the authors adopted two load profiles, one proportional to the masses and one obtained from the modal combination according to the Italian Standard regulation. The so-called uniform profile ($\mathbf{\Psi}$) proportional to the storey masses can be written as:

$$\mathbf{\Psi} = \mathbf{MI} \tag{3}$$

where $\mathbf{M}$ is the mass matrix and $I = [1, 1, \ldots, 1]^T$ is the unitary vector. Additionally, they adopted the Freeman distribution, square root of the sum squares (SRSS) distribution, based on spectral analysis, including the effect of the higher modes in the distribution of combined lateral loads. In this formulation, the distribution of lateral loads depends on the pseudo-acceleration spectrum of each mode S_a^m according to the following relationship:

$$\Psi_i = \sqrt{\sum_{m=1}^{N_m} F_{mi}^2} = \sqrt{\sum_{m=1}^{N_m} \Gamma_m \phi_{mi} m_i (S_a^{(m)})^2} \tag{4}$$

where Ψ_i is the ith component of the $\mathbf{\Psi}$ vector proportional to the load pattern, N_m the number of modes to excite at least 85% of the total mass, F_{mi} the shear at the ith plane of the mth mode determined by linear analysis on the response spectrum, m_i is the mass of the ith plane, ϕ_{mi} the mth mode shape at the ith plane, $S_a^{(m)}$ the mth pseudo-acceleration spectral mode and Γ_m the mth modal participation factor defined as

$$\Gamma_m = \frac{\phi_m^T M}{\phi_m^T M \phi_m} \tag{5}$$

In both load profiles, the transition from an MDOF system to its SDOF equivalent is not straightforward and does not exist shared assumptions. In conventional pushover analysis with a load profile proportional to the first mode, the force and displacement are scaled with the modal participation factor of the first mode (Γ_1) as follows.

$$a_C = \frac{V_b}{M\alpha_1} \quad \text{with} \quad \alpha_1 = \Gamma_1 \frac{\phi_1^T MI}{M} \tag{6}$$

where a_C is the acceleration capacity, V_b the base shear, M the total mass of the structure and α_1 the modal mass coefficient of the first mode.

$$d_C = \frac{D_t}{\Gamma_1 \phi_{1t}} \tag{7}$$

where d_c is the displacement capacity, D_t is the top storey displacement, and ϕ_{1t} is the modal component of the first mode corresponding to the top floor.

Yet, this approach cannot be considered reliable in the current application due to the absence of a unique representative fundamental mode. Additionally, there is no official recommendation in the Italian code for assessing the transformation factor Γ from MDOF to SDOF (Pinho et al. 2019).

Table 6 compares five methods for assessing the transformation factor in the x-direction which are largely adopted by practitioners and researchers. The first, labeled first mode, corresponds to the modal participation factor of the first mode. The second, named average, is the average of all the modal participation factors, while the third is the weighted average, with weights of the participation masses. The fourth, following the load profile assumption, is the SRSS of all modal participation factors. The fifth, named load distribution and proposed in this research, is obtained as follows:

$$\Gamma_{ld} = \frac{\phi_{lp}^T M}{\phi_{lp}^T M \phi_{lp}} \tag{8}$$

where ϕ_{lp} is the displacement pattern obtained in the linear field, assuming a load profile proportional to Ψ in Eq. 4 with SRSS combination or from a uniform profile proportional to the storey masses. In other words, due to the fact that no unique fundamental mode can be obtained, the seismic response directly obtained from the pushover analysis is a candidate for being the most representative of the real structural behavior of the building since it involves all the significant vibration modes of the structures.

More in detail, once the uniform profile proportional to the storey masses is obtained (refers to Fig. 12a) the corresponding displacement profile derived from the adopted load distribution can be assessed (see Fig. 12b).

Because of the no diaphragmatic behavior, the final vector $\phi_{i,eq}$, at each deck of the building, is obtained by simply computing an average of the displacements exhibited by the control points of all the frames along the x and y-direction, respectively (depending on the direction for which the pushover is performed). This operation makes sense since the discrepancies among all the control points lying on the same quote are negligible.

In conclusion, by adopting the proposed approach, the representativeness of the structural response, achieved by involving all the significant vibration modes, is maintained by assuming the displacement profile equivalent to the eigenvectors. Obviously, all the displacements have been scaled with respect to the maximum displacement experienced by the frame of competence in order to obtain the correct nondimensional form of the eigenvectors. Following this procedure, Γ_{ld} does not originate from the eigenvalue problem but from a rigorous analysis procedure.

Table 6 Comparison of the transformation factors (Γ) in the x-direction obtained from five approaches

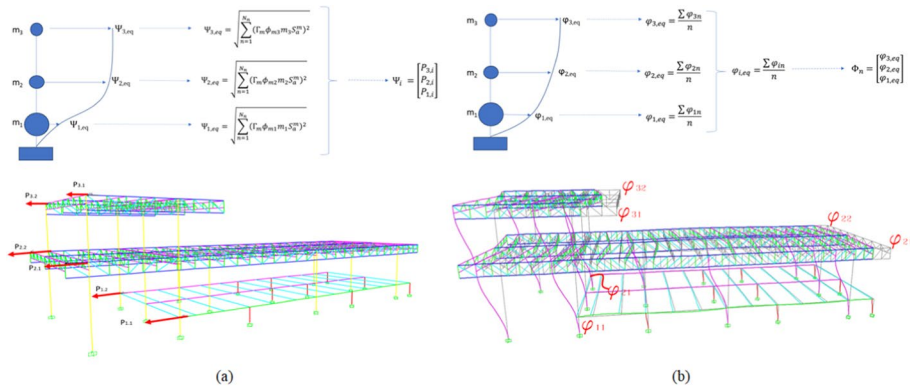| Method	Value
First mode (Γ_1)	2.107
Average (Γ_a)	1.608
Weighted average (Γ_{wa})	1.716
SRSS (Γ_{SRSS})	5.804
Load distribution-SRSS (Γ_{ld})	1.425
Load distribution-uniform (Γ_{ld})	1.532

Fig. 12 **a** Load profile obtained from SRSS combination of all the profile of forces proportional to each mode and **b** corresponding displacement profile when the building is pushed along the x-direction

The transformation factor corresponding to the mode participation factor for the first mode is approximately 2, which cannot be considered acceptable. This value reduces to an average of 1.6, implying that estimates using the first mode are more conservative than those derived from averages or weighted averages. However, when adopting the SRSS method and following the logic of the load pattern, the transformation factor increases significantly, reaching almost 6. This means that transitioning from MDOF to SDOF could lead to a substantial loss in capacity, resulting in an overly conservative design. Therefore, while the first two methods do not align with the assumed load profile, the fourth, although derived from SRSS, is excessively large. As a result, the authors chose a transformation factor related to load distribution, the smallest among the five options, which does not unduly compromise the capacity of the equivalent SDOF. The deformed configuration, after the application of the assumed load profile, is coherent with the idea behind the pushover analysis.

According to the National Building Code, the procedure for calculating vulnerability follows these steps: (1) obtain capacity curves for an MDOF system; (2) calculate the transformation factor and equivalent mass of the SDOF system; (3) transform the MDOF system into an SDOF system. (4) Determine the performance point of the structure and verify if it exceeds the minimum limit established by the regulations.

Figure 13 displays the load distribution assumed in the pushover analysis in the *x* and *y* directions for the two methods, one with loads proportional to the storey masses (uniform) and one multi-modal, from SRSS mode combination (SRSS).

In the *x*-direction, the load pattern is mainly unaffected by the method chosen for determining the force distribution, be it uniform or SRSS. However, in the *y*-direction, there are notable differences. The uniform method concentrates most of the force at the first level, which is the heaviest. In contrast, SRSS allocates most of the force to the mid-storey.

The observed differences are also tied to how the exoskeletons connect with the main structure in these two orthogonal directions. In the *x*-direction, they attach to the structure, concentrating the forces at the + 1.15 m level. Conversely, in the *y*-direction, the force concentration occurs at the + 6.15 m level. This distinct behaviour in force distribution in the *y*-direction suggests that one condition might be more adverse than the other.

Table 7 presents the relative values of load vectors for both uniform and SRSS distributions in the *x* and *y* directions. These relative values indicate the proportion of total
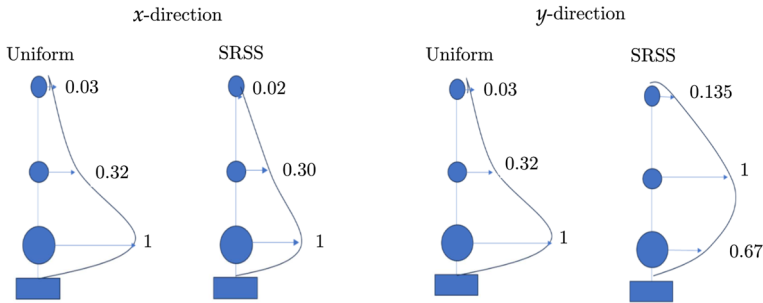
Fig. 13 Load distribution in the x and y directions for the two methods, one with loads proportional to the storey masses (uniform) and one, multi-modal, from SRSS mode combination (SRSS)

Table 7 Values of the load vectors for the uniform and SRSS distribution in the x and y directions expressed as relative percentage values to the total load

	x-direction			y-direction				
Frame No.	Uniform	SRSS	Frame No.	Uniform	SRSS	Frame No.	Uniform	SRSS
1	0.01%	1.00%	1	0.36%	0.18%	20	4.18%	1.94%
2	4.97%	2.85%	2	0.64%	0.49%	21	2.10%	4.48%
3	1.35%	3.50%	3	0.83%	1.41%	22	2.67%	0.95%
4	4.16%	6.30%	4	1.35%	0.29%	23	2.48%	5.33%
5	3.09%	2.31%	5	4.55%	1.79%	24	5.69%	2.53%
6	3.08%	3.10%	6	2.17%	3.80%	25	2.87%	6.16%
7	0.74%	0.52%	7	1.24%	0.54%	26	2.37%	0.98%
8	11.49%	8.86%	8	3.40%	1.79%	27	2.91%	6.16%
9	18.54%	11.58%	9	2.60%	4.81%	28	6.04%	2.23%
10	8.24%	6.53%	10	1.34%	0.36%	29	3.00%	6.16%
11	3.73%	9.54%	11	2.87%	1.15%	30	4.47%	1.51%
12	0.44%	0.67%	12	2.48%	4.80%	31	3.10%	6.16%
13	2.92%	3.85%	13	0.67%	0.57%	32	5.35%	2.02%
14	8.40%	9.11%	14	4.98%	3.09%	33	3.19%	6.06%
15	0.59%	0.26%	15	2.38%	4.80%	34	4.16%	1.21%
16	5.25%	3.42%	16	1.83%	0.37%	35	3.26%	5.90%
17	10.69%	8.44%	17	2.30%	1.12%	36	1.52%	0.98%
18	1.96%	2.00%	18	2.23%	4.64%	37	1.73%	2.97%
19	2.64%	6.66%	19	0.69%	0.26%			
20	1.05%	3.85%						
21	3.23%	1.89%						
22	0.30%	0.49%						
23	3.12%	3.28%						

shear force each frame bears to the overall base shears in the two orthogonal directions. In the x and y directions, the 23 and 37 plane frames experience uneven loading. This discrepancy is highlighted by colour-coded formatting, with green indicating the highest contributions and red signifying the lowest to the overall force. The most significant share of the total force is allocated to frame No. 9 in the x direction and frames No. 27 and 28 in the y direction. The frames at the perimeters are the least loaded, with some receiving a minimal contribution, even less than 0.01%. Notable differences between the Uniform and SRSS methods are observed in the y-direction. The uniform distribution generally allocates the load more evenly, while the SRSS distribution shows more significant variability among adjacent frames. This variability in the SRSS method is attributed to the complexity of the mode shape.

4.3 Seismic vulnerability assessment

The linear dynamic analyses revealed that the most vulnerable elements are the columns supporting the longest length roof span, which require specific care and need to be unloaded to achieve satisfactory seismic performance. Specifically, by adopting the scaling procedure described in Sect. 4.1, the first collapse of the building was detected when the building was subjected to 30% of the elastic spectrum. At this configuration, fundamental columns for the overall stability of the building exhibit DCRs largely over the safety threshold with safety ratios ranging from 1.2 up to 1.5. It follows that the pertinent vulnerability index obtained from linear dynamic analysis is $\zeta_E = 0.3$.

Interesting results could be provided by comparing the results obtained by the linear dynamic analysis with those from the Pushover analysis. In the following, the vulnerability index and the capacity curves obtained by following the procedure described in Sect. 4.2 will be shown.

Figure 14 displays the capacity curves of the structure as-built and with the seismic retrofitting in the x and y directions.

In the x direction, the as-built configurations of the uniform and SRSS load patterns show similar trends. Still, the uniform load pattern leads to slightly higher base shear values across all displacements. With the inclusion of exoskeletons, the difference becomes more pronounced, especially in the positive displacement range. The y-direction as-built reveals a notable distinction between the two load distributions. The uniform peaks quicker (lesser displacement) than the SRSS, revealing higher stiffness.
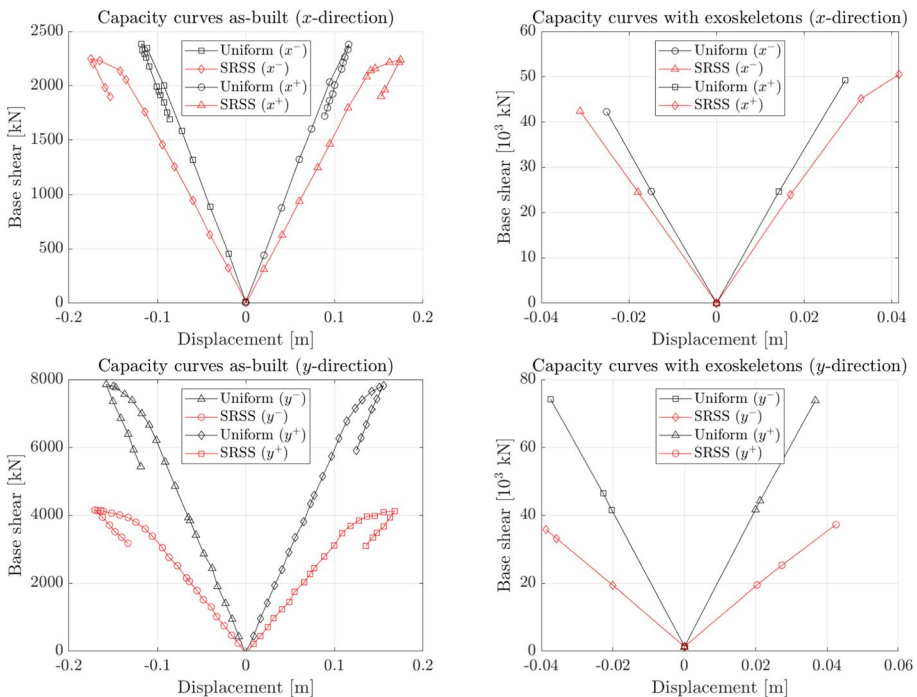

Fig. 14 Capacity curves of the structure as-built and with the seismic retrofitting in the x and y directions

When exoskeletons are integrated, the *y*-direction curves display a different trend. Both load patterns converge more closely in the positive displacement range, although distinctions still exist. Such difference recognized along the y-direction is strictly related to the different load distribution already discussed in Fig. 13.

Regarding capacity increment, the addition of exoskeletons leads to a manifest increase in the base shear capacity (nearly two orders of magnitude), especially in the positive displacement range.

Nonetheless, ductility, as inferred by the displacement range before reaching peak values, appears reduced with the exoskeletons. The as-built configuration, especially under SRSS load distribution, shows a broader displacement range, indicating more ductile behaviour. The as-built curves in the y-direction also reveal higher ductility when compared to the curves with exoskeletons. Once exoskeletons are integrated, the structures resist forces more rigidly, sacrificing some ductility for strength.

Integrating exoskeletons into the structure leads to a manifest increase in capacity in both directions. While this benefits the capacity, there is a trade-off in ductility, which appears to be reduced. Additionally, it should be remarked that the load distribution, either uniform or SRSS, plays a significant role in determining the capacity and ductility, with variations seen in both directions and configurations. Uniform distributions lead, in general, to a stiffer response with higher force peaks.

Table 8 resumes the parameters of the equivalent SDOF, specifically the mass m^* and the transformation factor.

The mass differences between the *x* and *y* directions reveal the structural asymmetry and the mass concentration in the *x* direction. Additionally, the transformation factors corresponding to a uniform distribution yield a slightly more conservative (higher) value than SRSS in both directions.

Figure 15 displays the acceleration displacement response spectrum (ADSR) verification for equivalent capacity curves of the SDOF system in both the *x* and *y* directions. The plots compare the elastic response spectrum with the behaviour of the structure under two load distributions (uniform and SRSS) and in two configurations (as-built and retrofitted with exoskeletons).

In the *x* direction, for both the as-built and retrofitted conditions, the uniform loading yields higher acceleration capacity than the SRSS loading. A similar trend repeats in the *y* direction.

As expected, the capacity of the retrofitted configurations is higher than the demand. Nonetheless, the retrofitted configurations generally exhibit reduced displacements compared to the as-built. This is related to the higher stiffness the exoskeletons provide, thereby reducing the displacement under the same loading. The effect of the load distribution is also evident: in the *x* direction, the uniform load distribution results in slightly larger displacements than the SRSS distribution for both configurations. This trend reverses in the *y* direction. As already observed in the results from the pushover analysis, the retrofitting improves capacity and reduces ductility. Additionally, it

Table 8 Equivalent SDOF parameters: mass (m^*) and transformation factor (Γ_{ld})

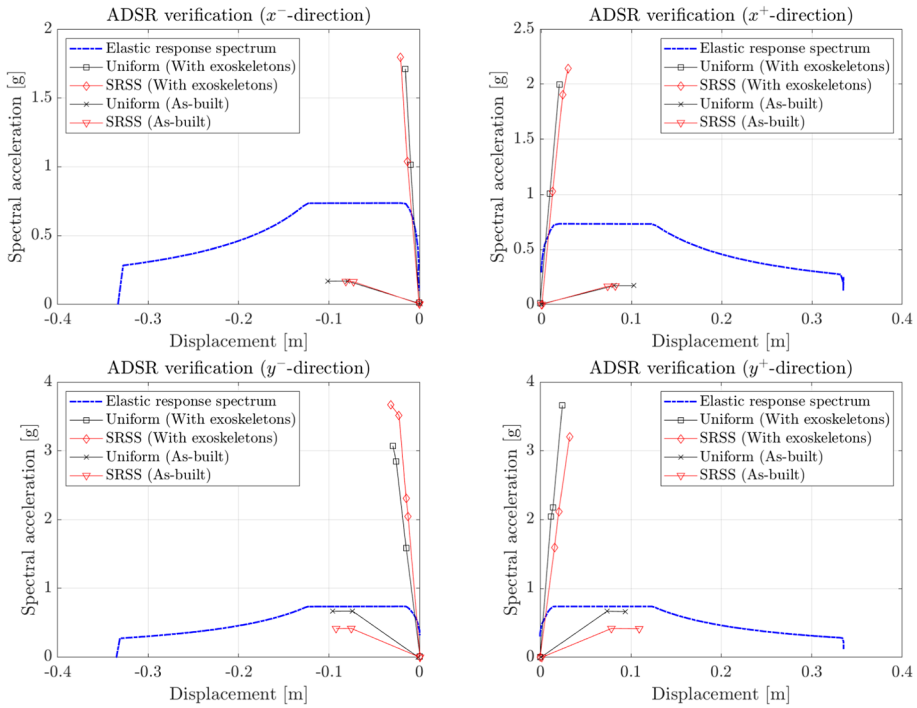| Parameter	x dir		y dir	
	SRSS	Uniform	SRSS	Uniform
m^* [ton]	1689	1668	926	1397
Γ_{ld}	1.43	1.50	1.29	1.50

Fig. 15 Equivalent capacity curves of the SDOF system in the ADSR (acceleration displacement response spectrum) plane in the as-built and retrofitted configuration with exoskeletons

should be noted that the less performing direction remains the *y* before and after seismic retrofitting.

Further considerations should be devoted in order to assess the structural efficiency of the exoskeletons and their capacity to capture the majority of the horizontal actions by unloading the existing structure. In Fig. 16, the values of the shear base of the structure
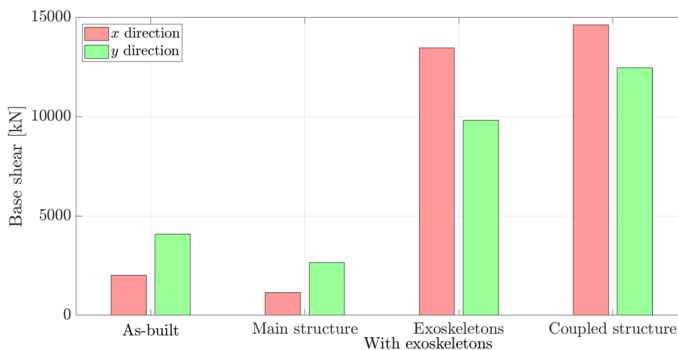
Fig. 16 Shear base of the no-retrofitted structure, the shear base of the coupled system splits between the reference structure and the exoskeletons and the total shear base of the retrofitted structures respect to **a** X and **b** y-direction

before and after interventions have been reported. In both directions, a dramatic reduction of the shear base close to 50% has been experienced by the retrofitted structure. Specifically, more than 80% of the total shear base has been captured by the exoskeletons. However, it is worth noting that after the introduction of the retrofitting solution, the total shear base increases from 2009 up to 14,610 kN in the x-direction and from 4090 to 12,456 kN in the y-direction. As mentioned before, such a significant increase is proportional to the increase of the extra stiffness provided by the exoskeletons as well as an increase in the seismic demand.

Table 9 resumes the numerical results of the pushover analyses. Following the nomenclature of the Italian Building Code, the table reports the maximum displacement capacity of the MDOF system ($d_{e,max}$), the ultimate (d_u^*) and yielding (d_u^*) displacements of the equivalent bi-linear capacity curve of the SDOF system, together with the behaviour factor of the SDOF system (q^*) and the vulnerability index ζ_E, estimates as the ratio between displacement capacity and demand of the SDOF oscillator.

All aspects highlighted in the comment of Fig. 15 can be quantitatively assessed from Table 9, which confirms the main aspects of such retrofitting: increased capacity, reduced stiffness and reduced ductility. Additionally, it is worth noting that a significant discrepancy can be observed by comparing the vulnerability index ζ_E obtained by the Pushover analysis (e.g. the smallest value among all the different profile loads' directions) and that one derived from the Linear Dynamic Analysis. As expected, the latter leads to more conservative results mainly due to the application type of the load profile as well as it does not take into account the correct plastic hinges placement along the

Table 9 Numerical results of pushover analyses for the MDOF system following the Italian Building Code nomenclature

Parameters	Scenario	Uniform				SRSS			
		x^+	x^-	y^+	y^-	x^+	x^-	y^+	y^-
$d_{e,max}$ [m]	As-built	0.201	0.209	0.120	0.080	0.199	0.208	0.129	0.080
	With exoskeletons	0.007	0.008	0.006	0.006	0.006	0.006	0.006	0.006
d_u^* [m]	As-built	0.082	0.101	0.100	0.091	0.081	0.101	0.093	0.094
	With exoskeletons	0.023	0.022	0.033	0.030	0.019	0.017	0.033	0.030
d_y^* [m]	As-built	0.073	0.081	0.077	0.073	0.072	0.080	0.077	0.073
	With exoskeletons	0.023	0.022	0.033	0.030	0.019	0.017	0.033	0.030
q^*	As-built	1.118	1.253	1.391	1.193	1.126	1.265	1.209	1.232
	With exoskeletons	1.000	1.000	1.100	1.000	1.000	1.000	1.100	1.000
Pushover									
ζ_E	As-built	0.409	0.483	0.832	1.088	0.408	0.484	0.718	1.122
	With exoskeletons	3.000	2.800	4.000	4.800	3.400	2.800	4.000	4.800
Linear dynamic analysis									
ζ_E	As-built	0.290							
	With exoskeletons	1.500							

Displayed values include the maximum displacement capacity $d_{e,max}$, the ultimate d_u^* and yielding d_y^* displacements of the equivalent bilinear capacity curve for the SDOF system, the behaviour factor q^*, and the vulnerability indices ζ_E, obtained by the two performed analysis, determined as the ratio of displacement capacity to demand for the SDOF oscillator. Data is differentiated by 'as-built' and 'with exoskeletons' scenarios and presented for both uniform and SRSS loading in the *x* and *y* directions

incremental step-by-step analysis. Finally, although the structure does not possess significant plastic capacity, this aspect plays a crucial role in the final vulnerability assessment of the retrofitted building.

The main consequence, as illustrated in Fig. 17, is that an increase in stiffness leads to a shift of the fundamental period from the right to the left side of the spectrum, characterized by higher acceleration demand.

Implementing exoskeletons for retrofitting underscores the complexities of attempting to reduce seismic demand. Introducing exoskeletons significantly increases stiffness, leading to a leftward shift in the modes of the elastic response spectrum, potentially increasing demand. Thus, retrofitting primarily enhances capacity without necessarily improving ductility or decreasing demand. In terms of seismic demand, merely adding minimal stiffness to reduce demand is counterproductive. It results in a considerable rise in demand, corresponding to the plateau of the elastic response spectrum. However, by significantly increasing stiffness, the structure can be positioned below the plateau. This ensures the coupled system mitigates the final seismic demand exerted on the main structure. It is crucial to note that maintaining the structure within the elastic range aligns with its intended function of remaining operational after seismic events. While staying in this range may cause higher demands, it aligns with the anticipated outcomes. Moreover, the manifest stiffness difference between the exoskeletons and the main structure results in the exoskeletons bearing most seismic forces, leaving the main structure largely unaffected. It should be outlined that the *x*-direction has been identified as the most critical in this context.
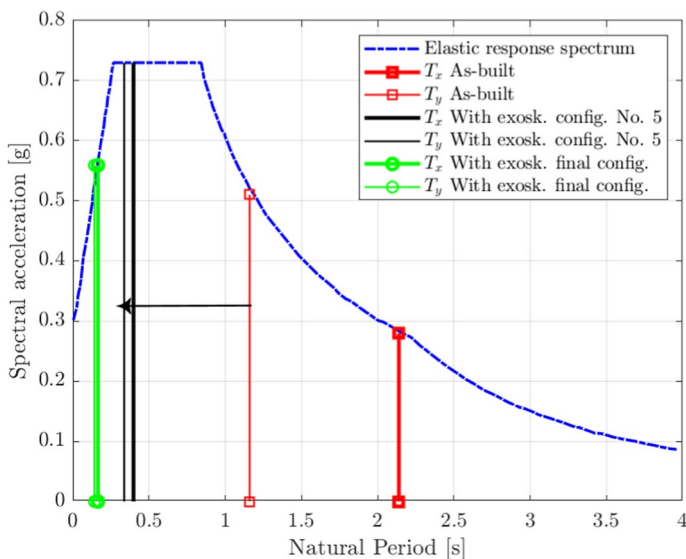

Fig. 17 Elastic response spectrum indicating the fundamental period in the *x* direction before and after retrofitting

5 Conclusions

This paper presents a comprehensive assessment of the seismic vulnerability of Foggia Airport (Italy) and an innovative seismic retrofitting solution using 3D arch exoskeletons. The primary objective was the evaluation of the seismic safety of the structure following the Italian Building Regulation.

The initial phase entailed an extensive review of historical records, technical drawings, and material testing to achieve an LC2 knowledge level. Then, the authors carried out a nonlinear pushover analysis based on a nonlinear FE model of the structure. A vital element of this evaluation was adopting a proper factor Γ to transform the multi-degree-of-freedom into the single-degree-of-freedom system. Different methods were compared, and the proposed approach for this research was derived from a preliminary static analysis under the assumed load profiles, one proportional to the storey masses (uniform) and one obtained from the SRSS mode combination (square root of the sum of the squares).

The analyses revealed that the airport does not fulfill the seismic safety criteria. To address this, 3D trussed arch exoskeletons have been added for seismic retrofitting. This solution proved effective, as the external exoskeleton system offloaded nearly 50% of the structural load, ensuring its safety during seismic events.

The main aspects of such retrofitting are increased capacity, reduced stiffness and reduced ductility. Most importantly, exoskeletons increase stiffness, causing a leftward transition of the modal response in the elastic response spectrum. Therefore, while retrofitting improves capacity, it reduces ductility and may increase seismic demand. Still, a substantial rise in stiffness enabled the positioning of the structure beneath the plateau in the elastic response spectrum, ensuring the coupled system also has a reduced seismic demand.

Additionally, keeping the structure within the elastic spectrum is consistent with its purpose of remaining functional after seismic actions. In conclusion, this research not only underscores the potential of 3D arch exoskeletons in enhancing seismic resilience but also highlights the challenges associated with their seismic evaluation using nonlinear static pushover analysis.

Declarations

Conflict of interest The authors declare that they have no known competing financial interests or personal relationships that could have appeared to influence the work reported in this paper.

References

Afsar Dizaj E, Salami M, Kashani M (2023) Seismic vulnerability analysis of irregular multi-span concrete bridges with different corrosion damage scenarios. Soil Dyn Earthq Eng. https://doi.org/10.1016/j.soildyn.2022.107678

Amini M, Poursha M (2018) Adaptive force-based multimode pushover analysis for seismic evaluation of midrise buildings. J Struct Eng (United States). https://doi.org/10.1061/(ASCE)ST.1943-541X.0002070

Antoniou S, Pinho R (2004) Development and verification of a displacement-based adaptive pushover procedure. J Earthq Eng 8(5):643–661. https://doi.org/10.1080/13632460409350504

Barbagallo F, Bosco M, Licciardello E, Marino EM, Rossi PP (2022) Design of steel exoskeleton equipped with BRBs for seismic upgrading of RC frames. Open Constr Build Technol J. https://doi.org/10.2174/18748368-v16-e2201060

Bellini O, Marini A, Passoni C (2018) Adaptive exoskeleton systems for the resilience of the built environment. TECHNE J Technol Archit Environ. https://doi.org/10.13128/Techne-22120

Bergami AV, Nuti C, Lavorato D, Fiorentino G, Briseghella B (2020) IMPAβ: incremental modal pushover analysis for bridges. Appl Sci 10(12):4287

Calvi G, Moratti M, O'Reilly G, Scattarreggia N, Monteiro R, Malomo D, Calvi P, Pinho R (2019) Once upon a time in Italy: The tale of the Morandi bridge. Struct Eng Int 29(2):198–217. https://doi.org/10.1080/10168664.2018.1558033

Caverzan A, Lamperti Tornaghi M, Negro P (2016) Taxonomy of the redevelopment methods for non-listed architecture: from façade refurbishment to the exoskeleton system. In: Proceedings of the Safesust workshop, JRC, conference and workshop reports.

Chen Z, Chui Y, Ni C, Doudak G, Mohammad M (2014) Load distribution in timber structures consisting of multiple lateral load resisting elements with different stiffnesses. J Perform Constr Facil. https://doi.org/10.1061/(ASCE)CF.1943-5509.0000587

Chopra A, Goel R (2002) A modal pushover analysis procedure for estimating seismic demands for buildings. Earthq Eng Struct Dyn 31(3):561–582. https://doi.org/10.1002/eqe.144

Collura D, Nascimbene R (2023) Comparative assessment of variable loads and seismic actions on bridges: a case study in Italy using a multimodal approach. Appl Sci 13(5):2771

Cucuzza R, Domaneschi M, Greco R, Marano GC (2023) Numerical models comparison for fluid-viscous dampers: performance investigations through genetic algorithm. Comput Struct 288:107122

Di Egidio A, de Leo A, Contento A (2023) Improvement of the dynamic and seismic response of non-structural rocking bodies through the ability to change their geometrical configuration. Eng Struct 275:115231

Di Egidio A, Pagliaro S, Fabrizio C (2021) Combined use of rocking walls and inerters to improve the seismic response of frame structures. J Eng Mech 147(5):04021016

Di Egidio A, Pagliaro S, Fabrizio C, de Leo AM (2020) Seismic performance of frame structures coupled with an external rocking wall. Eng Struct 224:111207

Di Lorenzo G, Colacurcio E, Di Filippo A, Formisano A, Massimilla A, Landolfo R (2020) State-of-the-art on steel exoskeletons for seismic retrofit of existing RC buildings. Int J 37:1–2020

e dei Trasporti M. d. I. (2008) Ntc2008–norme tecniche per le costruzioni. Technical Report DM 14/01/2008 [In Italian]

Fajfar P (1996) Towards a new seismic design methodology for buildings. University of Ljubljana, Slovenia

Fajfar P (2000) A nonlinear analysis method for performance-based seismic design. Earthq Spectra 16(3):573–592. https://doi.org/10.1193/1.1586128

Federal Emergency Management Agency (2006) Techniques for the seismic rehabilitation of existing buildings. Books Express Publishing, Berkshire

Foraboschi P, Giani H (2017) Exoskeletons: architectural and structural prerogatives (part i). Structural 214:1–23

Foraboschi P, Giani H (2018) Exoskeletons: seismic retrofit and architectural regeneration (part i). Structural 215:1–23

Formisano A, Messineo Y (2022) Seismic rehabilitation of abandoned RC industrial buildings: the case study of a former tobacco factory in the district of Avellino (Italy). Appl Sci 12(11):5705

Foutch DA, Hjelmstad K, Calderón EDV, Gutiérrez EF, Downs RE (1989) The Mexico earthquake of September 19, 1985-case studies of seismic strengthening for two buildings in Mexico city. Earthq Spectra 5(1):153–174

Ghazal H, Mwafy A (2022) Seismic fragility assessment of an existing multi-span RC bridge equipped with risk mitigation systems. Buildings. https://doi.org/10.3390/buildings12070982

Görgülü T, Tama YS, Yilmaz S, Kaplan H, Ay Z (2012) Strengthening of reinforced concrete structures with external steel shear walls. J Constr Steel Res 70:226–235

Habibi A, Izadpanah M, Namdar Y (2022) A new modal lateral load pattern for improving pushover analysis to estimate nonlinear responses of structures. Aust J Struct Eng 23(4):289–302

Humar J (2012) Dynamics of structures. CRC Press, Boca Raton

Kalkan E, Kunnath S (2006) Adaptive modal combination procedure for nonlinear static analysis of building structures. J Struct Eng 132(11):1721–1731. https://doi.org/10.1061/(ASCE)0733-9445(2006)132:11(1721)

Kalkan E, Kunnath S (2007) Assessment of current nonlinear static procedures for seismic evaluation of buildings. Eng Struct 29(3):305–316. https://doi.org/10.1016/j.engstruct.2006.04.012

Kaltakci MY, Arslan MH, Yilmaz US, Arslan HD (2008) A new approach on the strengthening of primary school buildings in Turkey: an application of external shear wall. Build Environ 43(6):983–990

Kawashima K, Takahashi Y, Ge H, Wu Z, Zhang J (2009) Reconnaissance report on damage of bridges in 2008 Wenchuan, China, earthquake. J Earthq Eng 13(7):965–996. https://doi.org/10.1080/13632460902859169

Landolfo R, Formisano A, Di Lorenzo G, Colacurcio E, Di Filippo A (2021) Steel exoskeletons for RC buildings retrofit: project methodology and application to a case study. Ingenio

Malomo D, Scattarreggia N, Orgnoni A, Pinho R, Moratti M, Calvi G (2020) Numerical study on the collapse of the Morandi bridge. J Perform Constr Facil. https://doi.org/10.1061/(ASCE)CF.1943-5509.0001428

Mao J, Zhai C, Xie L (2008) An improved modal pushover analysis procedure for estimating seismic demands of structures. Earthq Eng Eng Vib 7(1):25–31. https://doi.org/10.1007/s11803-008-0786-y

Marini A, Passoni C, Belleri A, Feroldi F, Preti M, Metelli G, Riva P, Giuriani E, Plizzari G (2017) Combining seismic retrofit with energy refurbishment for the sustainable renovation of RC buildings: a proof of concept. Eur J Environ Civ Eng 26:1–20

Marini A et al (2014) Technology options for earthquake resistant, eco-efficient buildings in Europe. European Commission, Joint Research Centre Scientific and Policy Reports

Marini A, Belleri A, Feroldi F, Passoni C, Preti M, Riva P, Giuriani E, Plizzari G (2015) Coupling energy refurbishment with structural strengthening in retrofit interventions. In: Proceedings of the Safesust workshop.

Markou G (2021) A new method of seismic retrofitting cost analysis and effectiveness for reinforced concrete structures. Eng Struct. https://doi.org/10.1016/j.engstruct.2021.113083

Martelli A, Clemente P, De Stefano A, Forni M, Salvatori A (2014) Recent development and application of seismic isolation and energy dissipation and conditions for their correct use. Perspect Eur Earthq Eng Seismol 1:449–488

Mazzolani FM, Ivanyi M (eds) (2002) Refurbishment of buildings and bridges, Vol. 435. Springer Science & Business Media

NEHRP F (2006) Techniques for the seismic rehabilitation of existing buildings, FEMA 547. Building Seismic Safety Council for the Federal Emergency Management Agency

Nestovito G, Occhiuzzi A (2016) Implementation of smart-passive dampers combined with double concave friction pendulum devices to retrofit an existing highway viaduct exploiting the seismic early warning information. Eng Struct 120:58–74. https://doi.org/10.1016/j.engstruct.2016.04.026

Pang Y, Cai L, Zhong J (2020) Seismic performance evaluation of fiber-reinforced concrete bridges under near-fault and far-field ground motions. Structures 28:1366–1383. https://doi.org/10.1016/j.istruc.2020.09.049

Pinho R, Bianchi F, Nascimbene R (2019) Valutazione sismica e tecniche di intervento per edifici esistenti in ca. Maggioli editorial spa

Reggia A, Morbi A, Plizzari G (2020) Experimental study of a reinforced concrete bridge pier strengthened with HPFRC jacketing. Eng Struct. https://doi.org/10.1016/j.engstruct.2020.110355

Rosso MM, Asso R, Aloisio A, Di Benedetto M, Cucuzza R, Greco R (2022) Corrosion effects on the capacity and ductility of concrete half-joint bridges. Constr Build Mater 360:129555

Rowe RE, Walther R (1993) Comité Européen du Béton-Fédération Internationale du Béton. CEB-FIP MODEL CODE 1990.

Saiidi M, Sozen MA (1981) Simple nonlinear seismic analysis of R/C structures. ASCE J Struct Div 107(5):937–952

Salkhordeh M, Govahi E, Mirtaheri M (2021) Seismic fragility evaluation of various mitigation strategies proposed for bridge piers. Structures 33:1892–1905. https://doi.org/10.1016/j.istruc.2021.05.041

Sasaki K, Freeman S, Paret T (1998) Multimode pushover procedure (mmp) - a method to identify the effects of higher modes in a pushover analysis. In: Proceedings of the 6th U.S. national conference on earthquake engineering

Scattarreggia N, Salomone R, Moratti M, Malomo D, Pinho R, Calvi G (2022) Collapse analysis of the multi-span reinforced concrete arch bridge of Caprigliola. Eng Struct, Italy. https://doi.org/10.1016/j.engstruct.2021.113375

Wada A, Qu Z, Ito H, Motoyui S, Sakata H,Kasai K (2010) Seismic retrofit using rocking walls and steel dampers. In: Improving the seismic performance of existing buildings and other structures, pp. 1010–1021

Wallace J, Eberhard M, Hwang S-J, Moehle J, Post T, Roblee C, Stewart J, Yashinsky M (2001) Highway bridges. Earthq Spectra 17(SUPPL.):131. https://doi.org/10.1193/1.1586196

Wardhana K, Hadipriono F (2003) Analysis of recent bridge failures in the United States. J Perform Constr Facil 17(3):144–150. https://doi.org/10.1061/(ASCE)0887-3828(2003)17:3(144)

Xiang N, Goto Y, Alam M, Li J (2021) Effect of bonding or unbonding on seismic behavior of bridge elastomeric bearings: lessons learned from past earthquakes in China and Japan and inspirations for future design. Adv Bridge Eng. https://doi.org/10.1186/s43251-021-00036-9

Yen W-H (2002) Lessons learned about bridges from earthquake in Taiwan. Public Roads 65(4):20

Zanini M, Toska K, Faleschini F, Pellegrino C (2020) Seismic reliability of reinforced concrete bridges subject to environmental deterioration and strengthened with FRCM composites. Soil Dyn Earthq Eng. https://doi.org/10.1016/j.soildyn.2020.106224

Zucca M, Crespi P, Stochino F, Puppio M, Coni M (2023) Maintenance interventions period of existing RC motorway viaducts located in moderate/high seismicity zones. Structures 47:976–990. https://doi.org/10.1016/j.istruc.2022.11.135